s_o = film radius in the constant-with-height region
$\bar{s}$ = flux radius, defined by Equation (3)
T_o = dimensionless thickness, $(s_o - R)(\rho g/\mu u_w)^{1/2}$
$\bar{T}$ = dimensionless flux, defined by Equation (4) or (15)
u = vertical fluid velocity
u_w = wire withdrawal speed
x = vertical coordinate

Greek Letters

μ = viscosity
π = 3.14159
ρ = density
σ = surface tension at the liquid-gas interface

LITERATURE CITED

1. Derayagin, B. V., and A. S. Titiyevskava, *Dokl. Akad. Nauk. SSSR*, **50**, 307 (1945).
2. Goucher, F. S., and H. Ward, *Phil. Mag.*, 6th Ser., **44**, 1002 (1922).
3. Landau, L. D., and V. G. Levich, *Acta Physiochem. U. R. S. S.*, **17**, No. 1-2, 41 (1942).
4. Levich, V. G., "Physicochemical Hydrodynamics," Chapt. 12, Prentice Hall, New York (1962).
5. Tallmadge, J. A., Ontario Waste Treatment Conf., Ontario Water Res. Comm., Canada, **11**, 121 (1964).
6. ———, R. A. Labine, and B. H. Wood, *Ind. Eng. Chem. Fundamentals Quart.*, **4**, 400 (1965).
7. Van Rossum, J. J., *Appl. Sci. Res.*, **A7**, 121 (1958).
8. White, D. A., Ph.D. dissertation, Yale Univ., New Haven (April, 1965).
9. ———, and J. A. Tallmadge, *J. Fluid Mech.*, **23**, 325 (1965).
10. ————, *Chem. Eng. Sci.*, **20**, 33 (1965).

Manuscript received June 8, 1965; revision received October 25, 1965; paper accepted October 29, 1965.

Binary Physical Adsorption of Argon and Nitrogen on Fixed Beds of Activated Silica Gel

DAVID T. CAMP and LAWRENCE N. CANJAR

Carnegie Institute of Technology, Pittsburgh, Pennsylvania

The physical adsorption and desorption of argon and nitrogen on fixed beds of 18 × 20 mesh silica gel at —78.5°C. and 1 atm. have been studied. Binary mixtures containing 5.52, 10.34, 51.0, 90.16, 95.13 mole % nitrogen, as well as pure argon and pure nitrogen, were used. Superficial gas velocities were varied from 0.10 to 0.27 ft./sec. Concentration vs. time curves were obtained at bed depths of 5.3, 8.6, and 12.0 in.

Resistance to mass transfer from the gas stream to the outside surface of the particles was found to be negligible. The rate is limited due to mass transfer from the outside surface to the internal surface of the particle. The data were correlated by the integrated Rosen diffusion solution with $D = 9.60\ (10^{-8})$ sq.ft./sec. or alternatively, by the Hiester and Vermeulen integrated model with $k_p = 0.23$ sec.$^{-1}$.

Despite the industrial importance of physical adsorption, information necessary for the accurate design of fixed bed adsorbers is scarce. There is considerable uncertainty in the molecular mechanism of this phenomenon. The rate data that have been obtained in the past have been correlated, in general, in an empirical manner and therefore are of limited applicability. Furthermore, little has been done concerning the practical situation where there is appreciable adsorption of more than one component. This research was undertaken to determine the proper form of the rate equation to be expected when both components of a binary mixture are adsorbed to an appreciable extent. With such a rate equation, an equilibrium relationship for the distribution of material between the gas and adsorbed state, and a material balance, one can, either analytically or by numerical techniques compute breakthrough curves. This approach would place the design of such fixed-bed units on a more fundamental basis than the empirical scale-up techniques in current use.

Lawrence N. Canjar is at the University of Detroit, Detroit, Michigan.

EXPERIMENTAL PROCEDURE

Except for several modifications, the equipment was the same as that used by Geser (*1*). A schematic drawing of the apparatus is shown in Figure 1. Cylinders containing argon and prepurified nitrogen, as well as mixtures of these gases, were used. Minimum purities were 99.9% for argon and 99.996% for nitrogen. The available mixtures were analyzed as 4.87, 9.84, 49.0, 89.66, and 94.48% argon. In each run, two cylinders of gas were used, one pure and one a mixture. As shown in Figure 1, gas from either of the cylinders flowed in ¼-in. stainless steel tubing through the gas selector switch, metering valves, a rotameter, and then into a thermostat maintained at —78.5°C. by a bath of methylene chloride and dry ice. The gas was then cooled to the bath temperature by approximately 65 ft. of tubing and entered the adsorption cell.

It flowed first into a 15-in. long auxiliary adsorption tube connected to the base of the main part of the adsorption vessel. The gas then entered the main part which consisted of two 6-in. long adsorption tubes connected by three flanges, one at the effluent end of each adsorption tube. The auxiliary tube was longer than the main tubes to permit establishment of the profile shape. The vessel was sealed by beveled metal-

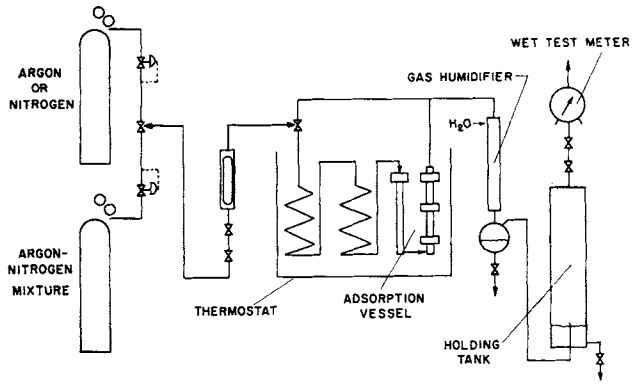

Fig. 1. Schematic diagram of apparatus.

to-metal joints gasketed with copper foil. As the gas left each adsorption tube, it passed through a 6-in. external cooler made of 3/16-in. stainless steel tubing to remove any possible heat of adsorption. After the gas left the adsorption vessel it passed through a gas humidifier column packed with glass beads and was saturated with water. Then it flowed through a wet test meter and was vented. Preliminary experiments indicated that the temperature rise in the bed would be less than 2°C. for all runs. Therefore, the bed could be assumed to be isothermal. It was also determined that the pressure drop through the system was negligible. All runs presented here were made at atmospheric pressure.

Eighteen by twenty mesh Davison 08 Grade silica gel was used as the adsorbent. It was activated by heating in an oven at 350°F. for approximately 24 hr. Two-mm. glass beads were used at each end of the adsorbent section in order to establish a flat velocity profile.

After the adsorption vessel was inserted into the thermostat approximately 2 hr. was required to reach thermal equilibrium. During this period dry nitrogen was fed through the system at a low velocity. When the system had come to thermal equilibrium the bed was saturated with a stream of either argon or nitrogen.

After the gas concentrations at all positions in the bed became constant, the gas selector switch was thrown, introducing a gas mixture to the system and marking the beginning of a run. During each run, flow rates were measured with the wet test meter. When the gas concentrations had leveled off at their new values, the run was complete. This procedure was then repeated to obtain a breakthrough curve for what might be termed the regeneration process. Runs were made at flow rates varying from 0.1 to 0.27 ft./sec.

Gas concentrations were measured at the exit of each adsorption tube by incorporating bead thermistors into a Wheatstone bridge and forming a thermal conductivity cell. One single-point self-balancing recording potentiometer was used to measure all three bridges. A switching system was programmed so that a reading was taken at each position every 10 sec.

DATA ANALYSIS

The raw potentiometer data were transferred to punched cards. Since the gas concentration was shown to be a linear function of the Wheatstone bridge output in the range studied, the data were easily converted to dimensionless concentrations. The thermistors did not respond instantaneously to changes in gas concentrations. Corrections were made for the resulting time lag by standard dynamic-analysis techniques. The derivatives $\left(\frac{\partial C}{\partial t}\right)_z$ and $\left(\frac{\partial^2 C}{\partial t^2}\right)_z$ were obtained by numerical differentiation.

The adsorption rate $\left(\frac{\partial q}{\partial t}\right)_z$ was evaluated from gas-concentration measurements by a differential material balance. Assuming constant plug flow and neglecting longitudinal and radial diffusion, one can write this balance as

$$\left(\frac{\partial q}{\partial t}\right)_z = \frac{F(c_o - c_i)}{A_x \rho_B}\left(\frac{\partial C}{\partial z}\right)_t + \frac{\epsilon(c_o - c_i)}{\rho_B}\left(\frac{\partial C}{\partial t}\right)_z \quad (1)$$

Because of the $\left(\frac{\partial C}{\partial z}\right)_t$ term, it is necessary to have breakthrough curves at a number of bed positions in order to apply this equation.

The equilibrium diagram, Figure 2, was obtained by evaluating Equation (2), which is based on an overall mass balance.

$$q_\infty - q_i = \frac{F(c_o - c_i)}{W_B}\int_o^\infty C\, dt \quad (2)$$

The integral in Equation (2) was corrected for the holdup in the gas line between the gas selector switch and the beginning of the adsorbent bed. Complete experimental data are contained in a thesis by Camp (2).

DISCUSSION

Figure 2 shows that both argon and nitrogen have almost linear equilibrium curves and that the total amount of gas adsorbed is, to a close approximation, independent of the concentration of the gas mixture in equilibrium with the adsorbent. All models considered assume the

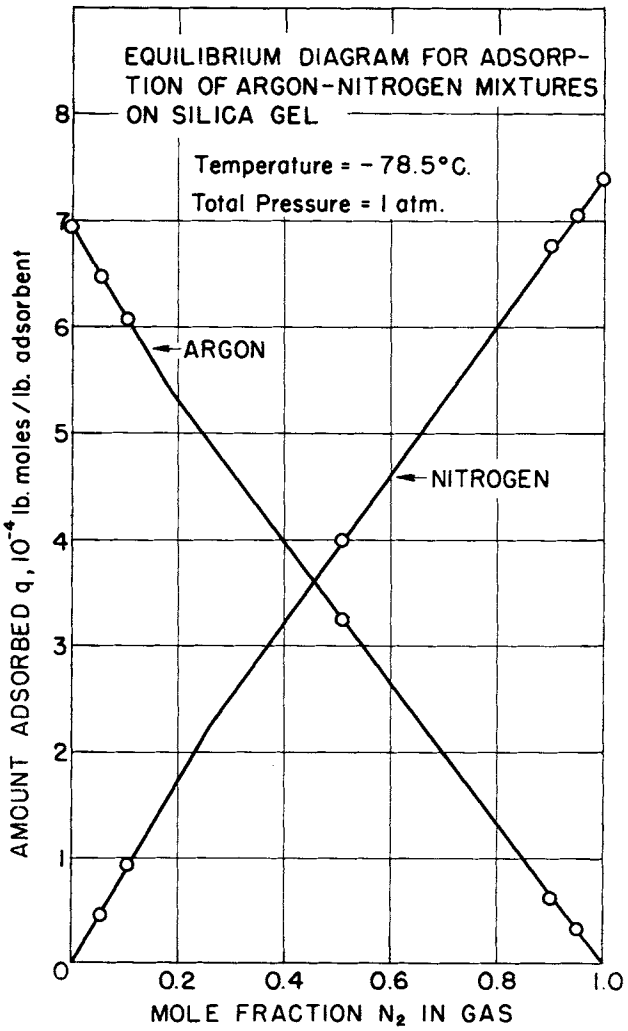

Fig. 2. Equilibrium diagram for argon-nitrogen mixtures adsorbed on silica gel.

volumetric flow rate F to be constant. Normally, this assumption is justified, because one is dealing with a dilute amount of adsorbable material in a relatively inert carrier gas. In this work the assumption of constant flow rate is valid because the total amount adsorbed is practically constant. Therefore, the adsorption of one molecule of argon is accompanied by the desorption of one adsorbed nitrogen molecule. This also explains the negligible heat effect noted earlier. This argon-nitrogen "molecular exchange" is mathematically equivalent to univalent ion exchange.

The overall mass transfer of adsorbate molecules from the gas phase to the adsorbent can be separated into the following steps:

1. Transfer from the gas phase to the external surface of the adsorbent (termed "external" mass transfer).
2. The surface reaction by which the molecule is adsorbed.
3. Surface diffusion of the adsorbed molecule from the external surface of the adsorbate to internal surface inaccessible to the bulk gas flow.
4. Diffusion of gas phase molecules through pores and interstices of the adsorbent prior to adsorption. (Steps 3 and/or 4 are termed "internal" mass transfer.)

The surface reaction is extremely rapid for physical adsorption. In addition, external mass transfer resistance was estimated by the correlation given by Hougen and Watson (*3*) and found to be negligible. Therefore, the overall adsorption process was limited by the internal mass transfer resistance.

A number of integrated solutions which predict gas and adsorbate concentrations as a function of time and bed position are available. To obtain such solutions, one must consider the material balance, the equilibrium relationship, the rate equation, as well as the boundary conditions. Hiester and Vermeulen (*4*) have adapted a solution proposed by Thomas (*5*), to be used where external or internal diffusion controls. By making certain substitutions of variables, they were able to put equations for internal or external mass transfer into the framework of the equation used by Thomas. To use this solution, one calculates

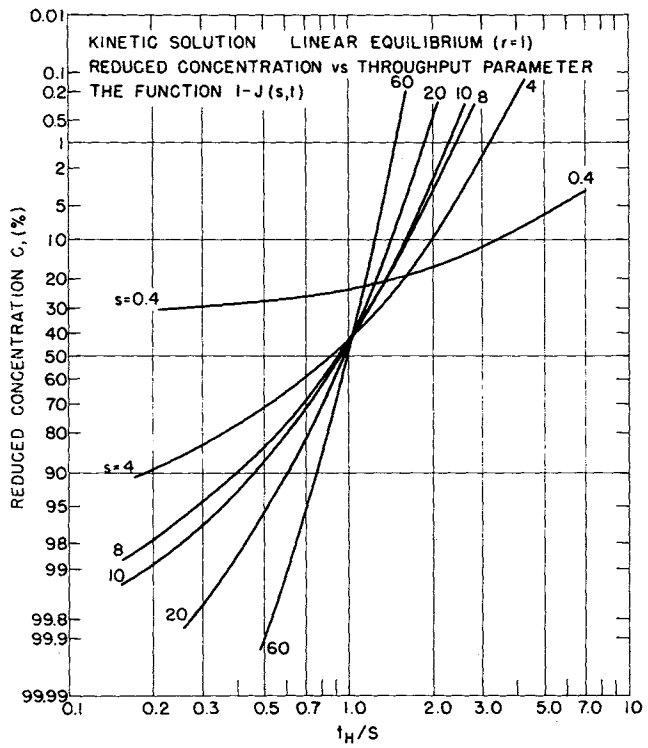

Fig. 3. Kinetic solution due to Hiester and Vermeulen.

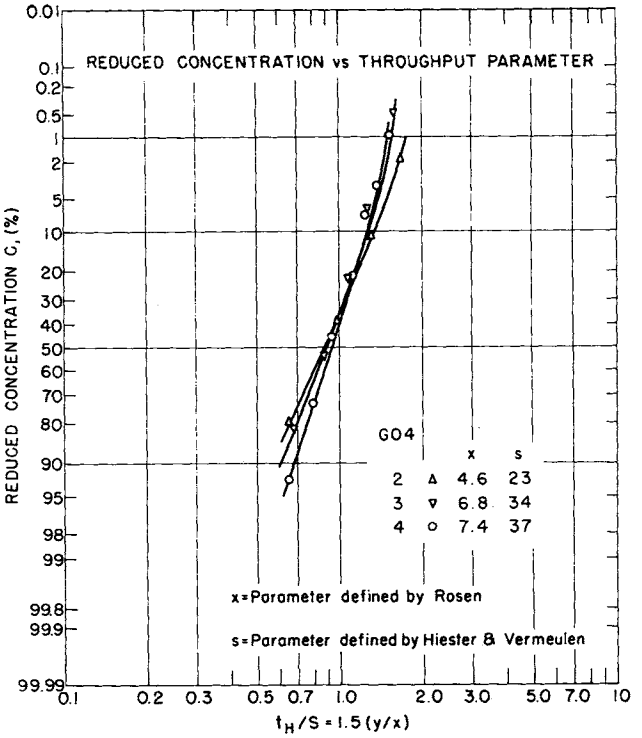

Fig 4. Experimental breakthrough curves for a typical run.

the throughput parameter, $t_H/s = c_o(V - v\epsilon)/q_\infty \rho_B v$. For the hypothetical case, where there are no diffusional effects and an infinite mass transfer rate, a step change in fluid concentration from c_i to c_o passes through the column unchanged in shape. The physical meaning of t_H/s can be illustrated by pointing out that, in this case, at any point in the bed, $c = c_i$ for $t_H/s < 1$ and $c = c_o$ for $t_H/s > 1$. However, if the resistance to mass transfer is present, breakthrough at a point occurs over a range of the parameter t_H/s, beginning when $t_H/s < 1$ and reaching completion at some $t_H/s > 1$. For linear equilibrium their parameter r equals unity. This solution

$$C = 1 - J(s, t_H) \tag{3}$$

is plotted in Figure 3 and can be used to determine $s = \kappa v\epsilon/F$, the column-capacity parameter.

If the solution given by Equation (3) is applicable, s, evaluated at any point in the bed, is constant throughout the run. In addition, its definition requires that it be proportional to v, the bulk-packed volume of adsorbent. A typical breakthrough curve is shown in Figure 4.

For internal mass transfer controlling, Hiester and Vermeulen have assumed that Equation (4) used by Glueckauf (*6, 7*) applies.

$$\left(\frac{\partial q}{\partial t}\right) = k_p\,(q^* - q) \tag{4}$$

κ is then related to k_p, the Glueckauf equation rate constant. In fact, for linear equilibrium

$$k_p = \kappa/D_G \tag{5}$$

A second integrated solution which is applicable is due to Rosen (*8, 9*). He used the diffusion equation to represent internal mass transfer and the film concept for external transfer. For the case of a linear equilibrium relationship between gas and adsorbent surface, he obtained a solution to the resulting partial integrodifferential equation by means of Laplace transforms and the corresponding inversion integral. In the experiments presented here, external resistance has been shown to be negligible.

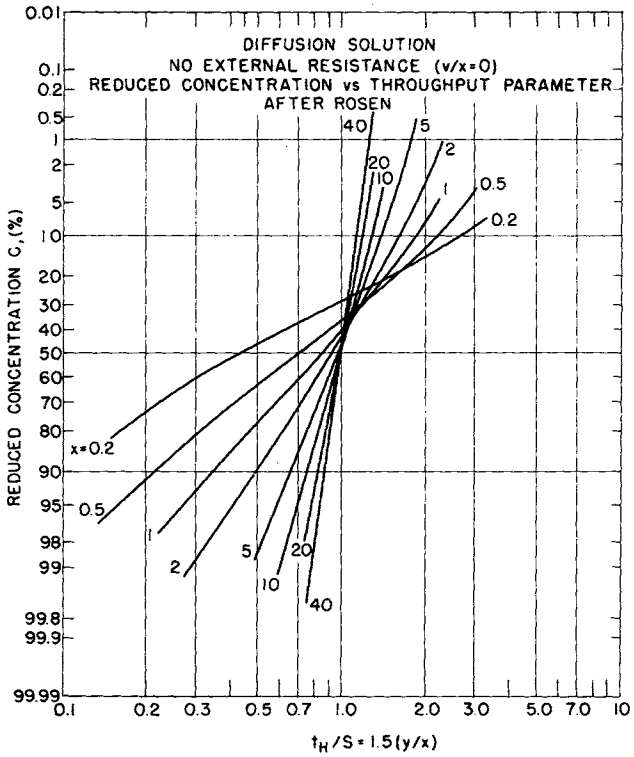

Fig. 5. Diffusion solution due to Rosen.

Therefore, Rosen's solution for this limiting condition is of particular interest. Figure 5 is a plot of this solution. The parameters x and y are related to the parameters s and t_H used in the solution due to Hiester and Vermeulen by the expression $t_H/s = 1.5\ y/x$. Glueckauf (6) has shown that for sufficiently large values of x and s the Rosen and Hiester and Vermeulen models give the same result with

$$k_p = \frac{60\ D}{D^2_p} \qquad (6)$$

or equivalently $s = 5x$. Comparison of Figures 3 and 5 indicates that, except for approximately the first 10% of the curve, the two solutions agree when $x > 2 (s > 10)$. In fact evaluation of the two solutions numerically shows that in this region the error is less than 1%. Virtually all the data obtained fell into this region and thus Equation (6) applies.

The diffusion coefficients were calculated from experimental breakthrough curves by a slope method. Figure 5 shows that for $x \geq 2$ and $0.70 \geq C \geq 0.05$ (breakthrough between 30% and 95% complete), the breakthrough curves are essentially linear when C is plotted against t_H/s on a probability vs. logarithmic scale. Experimental breakthrough data were corrected for response lags as already discussed and t_H/s calculated for each point. The transformation of concentrations to a probability scale was accomplished by determining a parameter u such that

$$\text{erf}\ (u) = 2\ (0.50 - C) \qquad (7)$$

A linear regression of u vs. $\ln(t_H/s)$ was performed for each breakthrough curve, considering those points for which both $((t_H/s) \geq 0.88)$ and $(C \geq 0.01)$, that is, the linear portion of the breakthrough curve. Correlation coefficients were typically at least 0.99, indicating that the data could be correlated extremely well by straight lines. Only those curves having three or more points in this region, about 75% of the total, could be properly evaluated by this technique.

Similarly, data obtained by evaluating the Rosen solution integral for ten values of x ranging from 0.5 to 20 were treated by this method and a table of slopes for these x values was determined. Then, slopes obtained from analysis of experimental breakthrough curves were compared with this table and the parameter x calculated by interpolation. Subsequent calculation of the diffusion coefficient D from x is straightforward.

These calculations were programmed for a digital computer and are summarized in Table 1. Data were obtained for fourteen pairs of initial and final gas concentrations and an average diffusion coefficient $D = (9.60 \pm 0.62)\ 10^{-8}$ sq.ft./sec. was calculated from groups 1 through 8.

Calculated diffusion coefficients for groups 9 through 14 varied considerably. Runs for which the initial gas concentration was lower in nitrogen content than the final gas concentration always gave higher values for calculated diffusion coefficients than runs made in the opposite direction. In fact, the larger the average diffusion coefficient for a particular group, the smaller the coefficient for the reciprocal group. The same effect can be observed in groups 1 through 8 but to a lesser degree.

Figure 2, the equilibrium diagram for the system, shows some curvature, adsorption of nitrogen being slightly

Table 1. Diffusion Coefficients Calculated from Experimental Data

Group	Gas concentration (Mole fraction nitrogen) Initial	Final	Diffusion coefficient, (sq.ft.)(sec.) × 10^8 Group avg.	95% confidence limits Low	High	No. of measurements
1	1.0000	0.9513	9.62	8.36	10.88	21
2	0.9513	1.0000	9.58	8.50	10.66	14
3	1.0000	0.9016	8.38	6.84	9.93	7
4	0.9016	1.0000	9.83	7.29	12.38	6
5	0.0000	0.0552	11.32	9.03	13.61	5
6	0.0552	0.0000	9.64	8.05	11.24	6
7	0.0000	0.1034	10.84	8.69	12.99	5
8	0.1034	0.0000	8.23	6.87	9.59	6
1-8			9.60	8.98	10.22	70
9	0.5099	1.0000	14.94	13.45	16.44	4
10	1.0000	0.5099	8.61	7.04	10.18	6
11	1.0000	0.0000	5.44	4.73	6.14	15
12	0.0000	1.0000	~30*			
13	0.5099	0.0000	6.81	5.73	7.90	9
14	0.0000	0.5099	16.06	11.00	21.13	3

* Breakthrough too fast to statistically evaluate slopes; estimated graphically.

favorable and conversely adsorption of argon unfavorable. This effect is naturally less of a factor for runs made with similar initial and final gas concentrations, for example groups 1 to 8. Table 1 indicates that the effect of curvature was indeed significant for those runs made with considerably different initial and final gas concentrations. The apparent increase in diffusion coefficient for runs in which there was a net adsorption of nitrogen is consistent with the favorable equilibrium curve for nitrogen. A similar argument applies for the smaller diffusion coefficients calculated for argon adsorption runs.

Almost all the runs of groups 1 through 8 could be divided into two sections on the basis of gas flow rate, one section having approximately twice the velocity of the other. The average diffusion coefficient and 95% confidence limits for the slow section were $(9.44 \pm 1.01)10^{-8}$ sq.ft./sec. The corresponding values for the fast sections were $(9.92 \pm 3.17)10^{-8}$ sq.ft./sec. The large spread for the latter section reflects the sensitivity of calculated slopes of steep breakthrough curves to small errors in concentration measurement.

Campbell (*10*) and Moison and O'Hern (*11*) have reported that their rate constants for internal diffusion increased with flow rate. The latter were working with liquids and believed the effect to be due to an increase in the effective surface area with flow rate during the transition from laminar to turbulent flow. Their Reynolds number was in the range 1 to 10, while in this work $2 < N_{Re} < 5$. Although the transition from laminar to turbulent flow is not as abrupt as in flow through tubes, for fixed beds $N_{Re} = 2$ is commonly considered the dividing line. However, the differences between the two sections reported here were not statistically significant at the 95% level. Therefore, a diffusion coefficient and confidence limits of $(9.60 \pm 0.62)10^{-8}$ sq.ft./sec. are reported for the combined sections.

A number of differential rate equations for internal mass transfer, including Equation (4), were also considered. In order to apply the experimental data to a rate equation, Equation (1) was used to calculate $\left(\frac{\partial q}{\partial t}\right)_z$. In practice, this method proved unsatisfactory because of inaccuracies introduced by the numerical differentiation required to obtain $\left(\frac{\partial C}{\partial z}\right)_t$. Breakthrough occurred very rapidly and resulted in large concentration differences between measuring positions at a given time. As a result, the differential rate data as calculated by Equation (1) from experimental measurements of gas concentration at various times and bed depths were not accurate enough to properly evaluate differential rate expressions.

It should be pointed out that this lack of required accuracy was not at all obvious. When calculated values of $\left(\frac{\partial q}{\partial t}\right)_z$ were correlated with Equation (4), the Glueckauf rate equation, the coefficient k_p was relatively constant for a large fraction of each breakthrough curve. For a time this was considered strong evidence that the numerical differentiation procedures were sufficiently accurate for analysis of the experimental data. However, k_p varied considerably for various runs and showed a marked increase as gas flow rate was increased, a result incompatible with the determination from the calculations showing fluid phase mass transfer resistance to be negligible and contrary to results obtained from the integral solution analysis. Furthermore, values as calculated from the Glueckauf equation were considerably less than those obtained from the integrated form of the equation. Considerable effort was expended in unsuccessful attempts to resolve these discrepancies on other grounds before it was found that breakthrough curves for various bed depths generated directly from the integrated form of this equation gave similar spurious effects when subjected to numerical differentiation procedures if the bed thickness was too large. As expected, the numerical procedures became more accurate as bed thickness decreased. More attention has been given to this problem in later work (*12*).

Therefore, while it might be argued that using the differential form of a mathematical model provides a more exacting test of experimental data, the results of these experiments could be more properly evaluated by using the integrated form of a rate equation.

While it is difficult to estimate k_p and D from the breakthrough data, it should be noted that this implies that the breakthrough curve is relatively insensitive to the value chosen for k_p or D. This is desirable if one has an estimate of k_p or D and wishes to predict breakthrough curves.

SUMMARY AND CONCLUSIONS

The adsorption and desorption of argon and nitrogen on fixed beds of silica gel at −78.5°C. and 1 atm. have been studied. It has been shown that:

1. Although this is clearly a case where both components are adsorbed, this particular system can be treated mathematically as one in which one component is being adsorbed and the volumetric flow rate is constant.
2. Internal mass transfer is controlling. This means that the overall mass transfer rate is determined by the transfer of molecules from the outside external surface of the particles to the interstices and pores within the particles.
3. The experimental data can be correlated by the integrated solutions of Hiester and Vermeulen with $k_p = 0.23$ sec.$^{-1}$ or by the integrated diffusion solution of Rosen with $D = 9.60(10^{-8})$ sq.ft./sec. Because of the sharpness of the breakthrough curves, differential rate expressions could not be adequately tested.

ACKNOWLEDGMENT

This research was supported by the National Science Foundation, the Esso Corporation, and the Ford Foundation. The authors are grateful for this assistance.

NOTATION

A_x = cross-sectional area of bed, sq. ft.
b = particle radius, ft.
c = gas concentration, lb.-moles adsorbate/cu. ft.
c_i = initial gas concentration, lb.-moles adsorbate/cu. ft.
c_o = final concentration, lb.-moles adsorbate/cu. ft.
C = reduced gas concentration, $(c_o - c)/(c_o - c_i)$, dimensionless
D = particle diffusion coefficient, sq. ft./sec.
D_G = ratio of concentrations on solid and in fluid phase at saturation, $q_\infty \rho_B / c_o \epsilon$, dimensionless
D_p = particle diameter, ft.
$\text{erf}(u)$ = the error function, $(2/\sqrt{\pi}) \int_o^u e^{-\beta^2} d\beta$
F = volumetric flow rate of gas through fixed solid, cu. ft./sec.
$I(s, t_H)$ = function used by Hiester and Vermeulen
k_p = rate constant, Glueckauf equation, sec.$^{-1}$
N_{Re} = Reynolds number, $\Phi D_p F\rho/6 \mu(1-\epsilon)A_x$, dimensionless
q = adsorbate concentration, lb.-moles adsorbate/lb. adsorbent
q_i = adsorbate concentration in equilibrium with c_i, lb.-moles adsorbate/lb. adsorbent
q^* = adsorbate concentration at interface, lb.-moles adsorbate/lb. adsorbent

q_∞ = adsorbate concentration in equilibrium with c_o, lb.-moles/lb. adsorbent
r = equilibrium parameter of Hiester and Vermeulen, dimensionless
s = column capacity parameter, $\kappa v\epsilon/F$, dimensionless
t = time, sec.
t_H = solution-capacity parameter, $\kappa(V - v\epsilon)/D_G F$, dimensionless
t_H/s = throughput parameter, $(V - v\epsilon)/D_G v\epsilon$, dimensionless
u = parameter defined by Equation (7)
v = bulk-packed volume of column, cu. ft. $v\epsilon$ is the void volume of the column
V = volume of gas fed to column, cu. ft.
W_B = weight of adsorbent bed, lb.
x = bed length parameter, $3D\ D_G v\epsilon/b^2F$, dimensionless
y = contact time parameter, $2D(V - v\epsilon)/b^2F$, dimensionless
z = bed depth, ft.

Greek Letters

ϵ = ratio of void space outside adsorbent particles to total volume of packed bed, dimensionless
κ = general rate coefficient, sec.$^{-1}$
μ = viscosity of gas, lb./(sec.)(ft.)
v/x = external resistance parameter of Rosen, dimensionless
ρ = fluid density, lb./cu. ft.
ρ_B = bulk density of bed, lb. adsorbent/cu. ft.
Φ = shape factor for nonspherical particles, dimensionless

LITERATURE CITED

1. Geser, J. J., and L. N. Canjar, *A.I.Ch.E. J.*, **8**, 494 (1962).
2. Camp, D. T., Ph.D. dissertation, Carnegie Inst. Technol., Pittsburgh, Pa. (1963).
3. Hougen, O. A., and K. M. Watson, "Chemical Process Principles," Pt. III, p. 987, Wiley, New York (1947).
4. Hiester, N. K., and Theodore Vermeulen, *Chem. Eng. Progr.*, **48**, 505 (1952). See also J. H. Perry et al., eds., "Chemical Engineers' Handbook," 4 ed., pp. 16-32, McGraw-Hill, New York (1963).
5. Thomas, H. C., *Ann. N. Y. Acad. Sci.*, **49**, 161-182 (1948).
6. Glueckauf, E., *Trans. Faraday Soc.*, **51**, 1540 (1955).
7. ———, and J. I. Coates, *J. Chem. Soc.*, 1315 (1947).
8. Rosen, J. B., *J. Chem. Phys.*, **20**, 387 (1952).
9. ———, *Ind. Eng. Chem.*, **46**, 1590 (1954).
10. Campbell, M. L., and L. N. Canjar, *A.I.Ch.E. J.*, **8**, 540 (1962).
11. Moison, R. L., and H. A. O'Hern, *Chem. Eng. Progr. Symposium Ser. No. 24*, **55**, 71 (1959).
12. Rimpel, A. E., Ph.D. dissertation, Carnegie Inst. Technol., Pittsburgh, Pa. (1964).

Manuscript received January 27, 1964; revision received October 12, 1965; paper accepted October 20, 1965. Paper presented at A.I.Ch.E. Memphis meeting.

Bubble Shapes in Nucleate Boiling

M. A. JOHNSON, JR., JAVIER DE LA PEÑA, and R. B. MESLER

University of Kansas, Lawrence, Kansas

An attempt is made to explain the differently shaped bubbles observed growing on a surface during nucleate boiling of water. Some of the bubbles photographed were very close to the spherical shape, while others were close to the hemispherical. Also, a number of bubbles had intermediate shapes and were called oblate bubbles.

Measurements of bubble dimensions and growth rates obtained from high-speed films were analyzed. By using a modified Rayleigh equation, the relative importance of the inertial and surface tension forces was computed. It appeared that the differences in shapes among bubbles can be explained on the basis of the relative importance of these forces.

It was found that for spherical bubbles inertial forces are small because of the slow growth rate and surface tension is clearly the dominant force. For hemispherical bubbles, however, the fast growth rate causes a very large inertial force which is greater than surface tension. For the oblate bubbles neither of the forces was found to be dominate and inertia as well as surface tension determines the shape.

In the understanding of nucleate boiling, a better knowledge of bubble behavior is desirable. Many aspects of the study of bubbles, such as growth rate, maximum size, and forces acting on a bubble, have been profusely studied by many different investigators. There has been no attempt, however, to explain the different shapes of bubbles growing on a surface, even though several authors have mentioned and photographed them. The forces acting on a bubble determine the bubble shape. Hence, a study of bubble shapes will probably be of great value in understanding the forces. The purpose of this paper is to call attention to this problem of bubble shapes, which the authors think has not been properly recognized, and to attempt an explanation of bubble shapes in their early stages of growth.

In the early studies of bubbles, spherical shapes were frequently assumed. High-speed photography has shown that this assumption is good in many cases. Shapes very close to the spherical have been reported by Roll (*13*), Keshock and Siegel (*9*) and others. However, Griffith (*3*), Gunther and Kreith (*4*), Han (*5*), Roll (*13*) and Chun (*2*) photographed bubbles that, at least at the early stages of growth, were far from being spherical.

The large number of possible shapes of bubbles growing on a plate may be classified as spherical, hemispherical, or oblate. Sequences of photographs illustrating the three different types of shapes are shown in Figure 1.

It should be mentioned at this point that the shapes predicted by the classical work of Bashforth and Adams (*1*) for static bubbles do not agree with the shapes photographed in this study. Bashforth and Adams obtained bubble shapes that are either nearly spherical or taller and narrower than the bubbles shown in Figure 1. As will be seen later, inertial forces are dominant during the early stages of growth of many bubbles. These forces were not taken into account by Bashforth and Adams and therefore